



# Runup uncertainty on planar beaches

Alec Torres-Freyermuth<sup>1</sup> · Jose Carlos Pintado-Patiño<sup>2</sup> · Adrián Pedrozo-Acuña<sup>3</sup> · Jack A. Puleo<sup>4</sup> · Tom E. Baldock<sup>5</sup>

Received: 11 March 2019 / Accepted: 5 September 2019 / Published online: 23 October 2019  
© Springer-Verlag GmbH Germany, part of Springer Nature 2019

## Abstract

Parameterization of wave runup is of paramount importance for an assessment of coastal hazards. Parametric models employ wave (e.g.,  $H_s$  and  $L_p$ ) and beach (i.e.,  $\beta$ ) parameters to estimate extreme runup (e.g.,  $R_{2\%}$ ). Thus, recent studies have been devoted to improving such parameterizations by including additional information regarding wave forcing or beach morphology features. However, the effects of intra-wave dynamics, related to the random nature of the wave transformation process, on runup statistics have not been incorporated. This work employs a phase- and depth- resolving model, based on the Reynolds-averaged Navier-Stokes equations, to investigate different sources of variability associated with runup on planar beaches. The numerical model is validated with laboratory runup data. Subsequently, the role of both aleatory uncertainty and other known sources of runup variability (i.e., frequency spreading and bed roughness) is investigated. Model results show that aleatory uncertainty can be more important than the contributions from other sources of variability such as the bed roughness and frequency spreading. Ensemble results are employed to develop a new parametric model which uses the Hunt (J Waterw Port Coastal Ocean Eng 85:123–152, 1959) scaling parameter  $\beta (H_s L_p)^{1/2}$ .

**Keywords** Runup · Uncertainty · RANS model · Swash zone · Parameterization

## 1 Introduction

Runup is defined as the wave-by-wave induced maximum water elevation measured on the foreshore above the mean ocean level. Runup is the result of the combination of the depth-integrated and time-averaged cross-shore momentum balance (i.e., setup) and wave-induced time-varying oscillations (i.e., swash motion). The swash oscillations can be decomposed further into high- and low-frequency components (Stockdon et al. 2006). The relevance of runup relies on the fact that it is often employed to define the level of exposure to inundation of any given beach, in relation to

its morphological features (e.g., Sallenger 2000; Stockdon et al. 2007). Ultimately, runup relative to the structure freeboard, or the deficit in runup freeboard, determines the risk and quantity of overtopping flows (Baldock et al. 2012). Hence, runup has an important role in coastal design parameters and risk reduction strategies, highlighting the need to develop reliable methods for its prediction.

Wave runup in the field is often collected using runup wires (Guza and Thornton 1982; Sallenger 1985; Holland et al. 1995; Hughes et al. 2014) or image-based techniques (e.g., Holman 1986; Ruessink et al. 1998; Ruggiero et al. 2004; Stockdon et al. 2006; Atkinson et al. 2017), with the latter being more common. For video imagery, cross-shore transects of pixel intensity are employed to track the water-land interface producing a runup time series. Swash statistics can be calculated from the mean-removed runup spectra (e.g., Stockdon et al. 2006) or from a wave-by-wave approach through time-series analysis (Hughes et al. 2014).

Extreme value statistics of runup are often defined as the vertical elevation exceeded by only 2% of the runup events (Holman 1986). Indeed,  $R_{2\%}$  is commonly correlated to beach slope and deep-water wave conditions in order to develop runup parameterizations (e.g., Holman 1986; Ruessink et al. 1998; Ruggiero et al. 2004; Stockdon et al.

---

This article is part of the Topical Collection on the *International Conference of Marine Science ICMS2018, the 3rd Latin American Symposium on Water Waves (LatWaves 2018), Medellin, Colombia, 19-23 November 2018 and the XVIII National Seminar on Marine Sciences and Technologies (SENALMAR), Barranquilla, Colombia 22-25 October 2019*

---

Responsible Editor: Alejandro Orfila

✉ Alec Torres-Freyermuth  
ATorresF@iingen.unam.mx

Extended author information available on the last page of the article.

2006; Brinkkemper et al. 2013; Atkinson et al. 2017). However, runup measurements are often scattered about empirical parameterizations (Guza and Feddersen 2012). For instance, Atkinson et al. (2017) assessed the accuracy of nine common runup parameterizations using field data from 11 different beaches along the Australian East coast and found no one model to be the best model on all beaches, with the best models yielding errors of order 25%. The large errors suggest either that parameterizations may be site dependent or the lack of key processes in their formulation.

Laboratory experiments (e.g., Baldock et al. 2000; Baldock and Huntley 2002; Baldock 2006; Palmsten and Splinter 2016, among many others) and numerical models (e.g., Madsen et al. 1997; Stockdon et al. 2014; Ruju et al. 2014; Fitzgerald et al. 2016; Fiedler et al. 2019, among many others) provide a means to study runup under a variety of forcing scenarios under controlled conditions. The advent of transient nonlinear swash models (e.g., Briganti et al. 2016) has increased the use of numerical models to improve runup parameterizations by incorporating further information regarding the environmental conditions, the wave forcing, and the beach geometry. For instance, Guza and Feddersen (2012) employed a Boussinesq-type model to investigate the effect of angular and frequency spread in infragravity swash and a new parameterization was derived in order to improve predictions of infragravity runup over idealized bathymetry during energetic wave conditions. Medellín et al. (2016) employed a non-linear shallow water equations (NLSWE) non-hydrostatic model [SWASH; Zijlema et al. 2011], to develop a site-specific parameterization that depends on wave conditions and tidal elevation. They found that accounting for tidal elevation improved the correlation coefficient between numerical and parameterised  $R_{2\%}$ . Atkinson et al. (2017) also found model accuracy varied with tidal stage. More recently, Park and Cox (2016) employed a Boussinesq-type numerical model to develop a new runup parameterization considering the berm width. It was found that including the berm width improved the predictions when compared with previous parametric models (e.g., Stockdon et al. 2006). Poate et al. (2016) derived a runup equation for a gravel beach incorporating the grain size that predicts the field data well. However, all the aforementioned laboratory and numerical runup studies often employed a single realization (deterministic approach), yielding a unique relationship between the wave/beach conditions and the  $R_{2\%}$  (Holman 1986).

Despite these advances in the understanding of the runup process, the reliability of the runup prediction in real field applications can be unreliable, as its estimation derived from empirical formulae or state-of-the-art models involves a certain amount of uncertainty from different sources (Atkinson et al. 2017). These uncertainties could

lead to errors in the prediction of extremes; therefore, further research should be aimed at understanding the influence of these uncertainties on the resulting engineering analysis (e.g., Rodriguez-Rincon et al. 2015). For instance, a few numerical studies have been devoted to quantifying uncertainty in runup estimations due to variations of parameters such as incoming wave height (Ge and Cheung 2011; Ricchiuto et al. 2014), shape of the incoming wave (Didenkulova et al. 2015), and friction coefficient (Ricchiuto et al. 2014). However, no previous study has investigated the uncertainty associated with random waves and its relative importance with respect to the other sources of runup variability (e.g., frequency spread and bed friction). Aleatory uncertainty can be estimated by conducting multiple model realizations, i.e., employing different forcing time series derived from the same spectral wave conditions. This stochastic approach has been recently adopted in coastal engineering for the study of wave-structure interaction (Williams et al. 2014; Palemón-Arcos et al. 2015; Romano et al. 2015).

This paper investigates, by means of a two-dimensional (2D) deterministic numerical model, the role of uncertainty in wave runup predictions and its relative importance when compared with other sources of variability. A Reynolds-averaged Navier-Stokes (RANS) approach is employed since NLSWE or Boussinesq models lack of all the physics that are fundamental to investigate uncertainty associated to the wave transformation processes. The outline of the paper is the following. In Section 2, the model employed in this study is described and validated with laboratory runup data. Then, the methodology employed in the present work and the description of the simulated cases is presented in Section 3. The ensemble predictions of setup, significant swash, and runup for the different cases corresponding to different forcing and beach conditions are presented in Section 4. Furthermore, a new parameterization for wave runup is obtained based on the numerical results. A discussion of the current results and how they are related with previous work is presented in Section 5. Finally, concluding remarks are provided in Section 6.

## 2 Model description

### 2.1 Numerical formulation

Accurate runup predictions require a fully dispersive wave model that simulates non-linear wave transformation including wave breaking, wave-induced setup, high- and low-frequency wave transformation, and swash-swash interactions. A depth- and phase-resolving model that solves the 2D Reynolds-averaged Navier-Stokes (RANS) equations with a turbulence closure and a free-surface

tracking scheme (COBRAS; Lin and Liu 1998; Hsu et al. 2002; Losada et al. 2008) is employed in this work to estimate runup. The COBRAS model solves the 2D RANS equations for an incompressible fluid given by,

$$\frac{\partial \langle u_i \rangle}{\partial x_i} = 0 \tag{1}$$

$$\begin{aligned} \frac{\partial \langle u_i \rangle}{\partial t} + \langle u_j \rangle \frac{\partial \langle u_i \rangle}{\partial x_j} = & -\frac{1}{\rho} \frac{\partial \langle p \rangle}{\partial x_i} + g_i \\ & + \frac{1}{\rho} \frac{\partial \langle \tau_{ij} \rangle}{\partial x_j} - \frac{\partial \langle u'_i u'_j \rangle}{\partial x_j} \end{aligned} \tag{2}$$

where  $t$  is time,  $x_i$  is the bed-parallel ( $i = 1$ ) and bed-orthogonal ( $i = 2$ ) coordinate,  $g_i$  is the gravitational acceleration component,  $u_i$  is the fluid velocity in direction  $x_i$ ,  $\rho$  is the fluid density,  $p$  is the pressure,  $\tau_{ij}$  is the shear stress, and angle brackets denote Reynolds-averaged quantities. The influence of turbulence fluctuations on the mean flow field is introduced via the Reynolds stresses  $\rho \langle u'_i u'_j \rangle$ , approximated using a  $k - \epsilon$  turbulence closure scheme. The governing equations for production of turbulent kinetic energy  $k$  and energy dissipation rate  $\epsilon$  are derived from the Navier-Stokes equations and correlations of turbulence fluctuations in the  $k$  and  $\epsilon$  equations are replaced by closure conditions. A non-linear algebraic Reynolds stress model is used to relate the Reynolds stress tensor and the strain rate of mean flow (Lin and Liu 1998; Rodi 1993) and the volume of fluid (VOF) method is used (Hirt and Nichols 1990) to track the free surface.

A rough-wall logarithmic law is imposed as the bottom boundary condition for velocity parallel to a solid boundary (Lin and Liu 1998). The bottom shear stress is expressed via a friction velocity,  $u_*$ , assuming that a logarithmic velocity profile is valid between the bottom and the half grid point above the bed as,

$$u_* = \frac{\kappa u (\Delta z_C / 2)}{\ln \left[ \frac{30 \Delta z_C / 2}{K_s} \right]} \tag{3}$$

where  $\kappa$  is the von Karman constant (0.4) and  $K_s$  is the apparent roughness that is set equal to  $2D_{50}$  (Hsu et al. 2006) for the median grain size  $D_{50}$ . These boundary conditions were deemed suitable for prediction of bed shear stress and runup distance during a dam-break-driven swash event with this numerical model (e.g., Torres-Freyermuth et al. 2013). This modelling approach has been employed in previous studies of swash zone processes, driven by a dam-break event, including the study of turbulent kinetic energy dissipation (Zhang and Liu 2008), bed shear stresses (Torres-Freyermuth et al. 2013), and bed boundary layer dynamics (Pintado-Patiño et al. 2015). However, the RANS model capability for the study of wave runup has not been investigated previously.

## 2.2 Model setup

The numerical model implementation to study runup processes requires the solution of the governing equations in a model coordinate system that is bed-parallel ( $x$ ) and bed-orthogonal ( $z$ ) owing to the partial cell treatment (e.g., Zhang and Liu 2008; Torres-Freyermuth et al. 2013) (see Fig. 1). A uniform grid of  $\Delta x = \Delta z = 0.015$  m was employed in this work for two different beach slopes (Fig. 1a, b). Previous studies reported a residual water layer that remains at the first grid point during the backwash phase (Torres-Freyermuth et al. 2013; Desombre et al. 2013) and hence the runup time series were extracted by tracking the water-land interface at two grid points above the bed.

The wave forcing in the numerical model considered second-order generation and active wave absorption (Torres-Freyermuth et al. 2010). Non-linear wave interactions were estimated following (Longuet-Higgins and Stewart 1960), where the free surface  $\eta$  and velocity potential  $\Phi$  are given by,

$$\eta = \zeta_1^{(1)} + \zeta_2^{(1)} + \zeta_{12}^{(2)} \tag{4}$$

$$\Phi = \phi_1^{(1)} + \phi_2^{(1)} + \phi_{12}^{(2)} \tag{5}$$

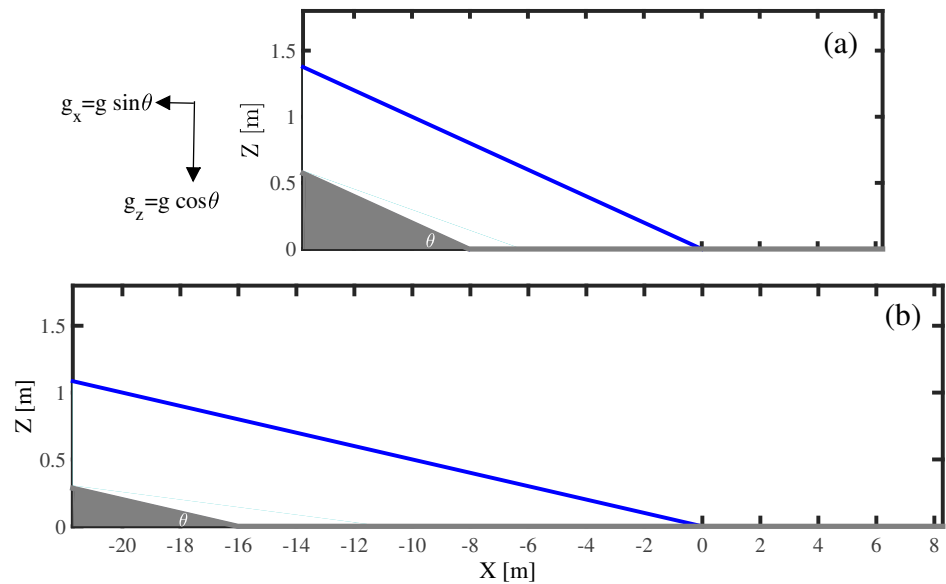
where the  $\zeta$  is the free surface elevation, the superscripts 1 and 2 denote the first- and second-order solutions respectively, the single subscripts denote individual wave components, and the double (i.e., 12) subscript corresponds to the difference (bound) wave interaction. A flux boundary condition is prescribed at the location of the most seaward sensor. For forcing the model, the measured free-surface elevation was band-passed ( $0.5f_p < f < 2f_p$ ; where  $f$  is frequency and subscript  $p$  denotes peak) and further decomposed into Fourier components. Thus, free-surface and velocity potential second-order solutions are given by a sum of primary and difference interactions between each pair of components as Baldock et al. (1996),

$$\eta = \sum_{n=1}^N \zeta_n^{(1)} + \sum_{n=1}^N \sum_{m=n+1}^N \zeta_{nm}^{(2)} \tag{6}$$

$$\Phi = \sum_{n=1}^N \phi_n^{(1)} + \sum_{n=1}^N \sum_{m=n+1}^N \phi_{nm}^{(2)} \tag{7}$$

Finally, second-order velocity components ( $u$  and  $w$ ) can be obtained by taking the derivative of the velocity potential. An active wave absorption is also implemented in the forcing boundary following (Torres-Freyermuth et al. 2010) in order to avoid re-reflection and ensure mass conservation within the computational domain.

**Fig. 1** Numerical setup of the simulated cases for the beach slopes **a**  $\beta = \tan \theta = 0.1$  and **b**  $\beta = \tan \theta = 0.05$ . The reference frame is oriented parallel and orthogonal to the beach face with a uniform mesh size, the blue line represents the still water level, and the gray shaded area is the seabed



### 2.3 Model validation

For the numerical model validation, we employed runup measurements corresponding to experiments for monochromatic waves (Baldock and Holmes 1999) and transient wave groups (Baldock 2006). The laboratory experiments were carried out in a wave flume 18 m long, 0.9 m wide, and 0.8 m deep. The experimental setup is described elsewhere (Baldock 2006) and hence an overview is given here.

The laboratory experiments employed a 1:10 planar beach ( $\beta = \tan \theta$ ) composed of rigid, smooth polyethylene beginning 5.65 m from the wave paddle. Waves were generated using a hydraulic-driven wedge-type paddle considering second-order generation for long waves (e.g., Baldock et al. 2000) and active wave absorption. Resistance-type wave gauges were located at different cross-shore locations outside and inside the surf zone. Moreover, the runup was acquired using a runup wire elevated 3 mm above the bed. The still water line (SWL) intersection on the beach face (as defined by the runup wire prior to the commencement of each test) defines the origin of the vertical coordinate for the runup data. The model setup follows the description in 2.2.

Baldock and Holmes (1999) conducted laboratory experiments on wave runup due to monochromatic waves. Four different wave conditions, comprising different values of the surf similarity parameter  $\xi_0 = \beta / (H_o / L_0)^{1/2}$  (Battjes 1974), were selected for the model-data comparison. The numerical model was forced with the wave forcing boundary condition described in Section 2.2 using the first-order solution. Despite the coarse grid resolution, the numerical model performance is satisfactory when compared against the runup wire data. The discrepancy between simulated and measured maximum runup increases with decreasing surf similarity parameter (differences of 1.6%, 4.0%, 13%, and

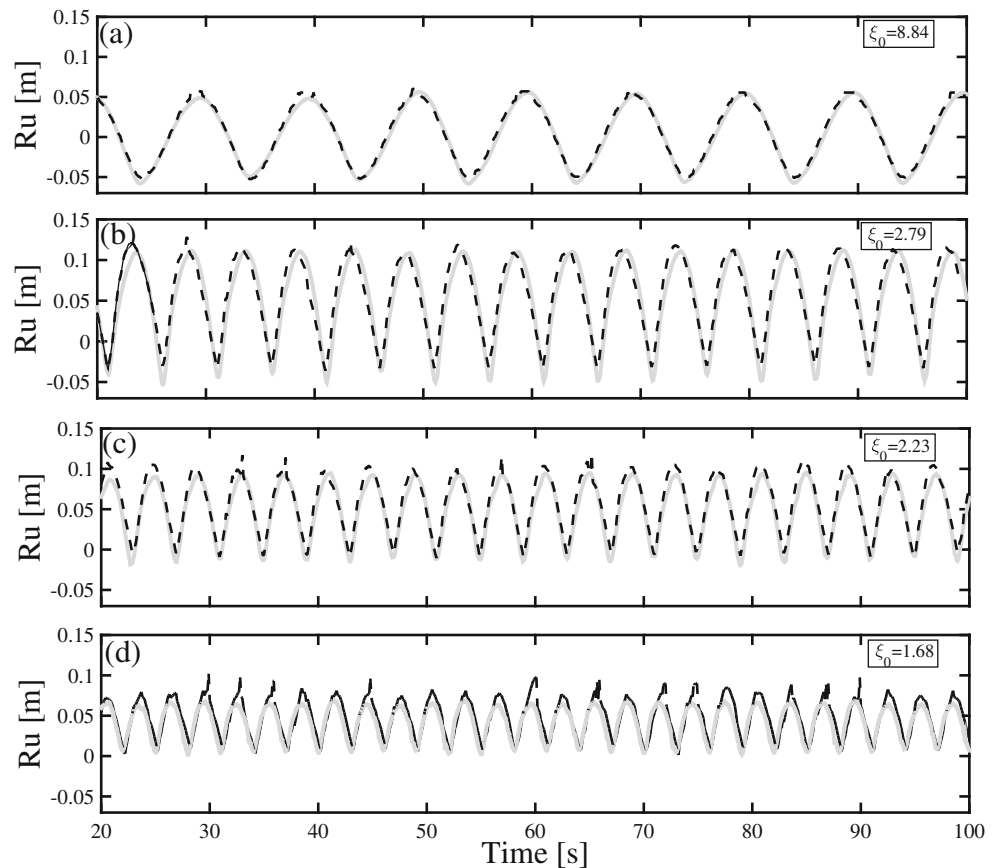
17%, respectively from top to bottom in Fig. 2). The model skill (Willmott et al. 1985) is employed to assess the model performance for the prediction of wave runup.

$$\theta_{skill} = 1 - \left[ \frac{\sum_{t_{ini}}^{t_{end}} (\theta_{pred,t} - \theta_{meas,t})^2}{\sum_{t_{ini}}^{t_{end}} (|\theta_{pred,t} - \overline{\theta_{meas,t_{ini:end}}}| + |\theta_{meas,t} - \overline{\theta_{meas,t_{ini:end}}}|)^2} \right], \quad (8)$$

where  $\theta_{meas}$  and  $\theta_{pred}$  represent the measured and predicted quantities as a function of time  $t$ . The model skill ranges from complete disagreement ( $\theta_{skil} = 0$ ) to perfect agreement ( $\theta_{skil} = 1$ ). Table 1 shows the model skill regarding time series of runup predictions for the simulated cases.

The numerical model was also validated against runup data corresponding to a focusing transient wave group experiment conducted by Baldock (2006). Numerical simulation of this data requires a fully dispersive and non-linear model to predict the wave focusing at intermediate water depth, the wave breaking, and the runup event associated to the breakpoint-generated low-frequency wave (Baldock 2006). Lara et al. (2011) investigated the mechanisms of low-frequency wave transformation under similar wave conditions inside the surf zone using the same numerical model, finding a satisfactory agreement with respect to data. However, an assessment on the model capability to predict wave-induced runup was not addressed in that study. Here, the numerical model was forced using second-order generation and active wave absorption in the rotated reference frame (Fig. 1a). The numerical model reproduces the forcing time series (Fig. 3a), predicts the shoaling (Fig. 3b), and wave focusing (Fig. 3c). Some discrepancies are observed near the wave-focusing location owing to the low mesh resolution employed for this work. Nevertheless, the extreme

**Fig. 2** Model-data (data: black dashed curve; model: gray solid curve) comparison of wave runup. Laboratory data correspond to the runup wire of Baldock and Holmes (1999) for: **a**  $H = 0.0212$  m,  $T = 10$  s, and  $\xi_0 = 8.84$ ; **b**  $H = 0.046$  m,  $T = 5$  s, and  $\xi_0 = 2.79$ ; **c**  $H = 0.05$  m,  $T = 4$  s and  $\xi_0 = 2.23$ ; **d**  $H = 0.05$  m,  $T = 3$  s, and  $\xi_0 = 1.68$



runup event, induced by the break-point generated low-frequency wave, is reproduced in the numerical model (Fig. 3d). It is worth noting that the model performance can be significantly improved by increasing the mesh resolution (not shown), but at the cost of a increase in the computational time. Thus, we employed the coarse resolution to conduct a parametric study.

**2.4 Simulated cases**

Previous studies pointed out the influence of frequency spreading ( $\gamma$ ) (e.g., Guza and Feddersen 2012) and bed roughness (Apotsos et al. 2008) on the infragravity swash and the wave-induced setup, respectively. The simulated cases in the present work (Table 2) consider different com-

binations of random wave forcing conditions ( $H_s, T_p, \gamma$ ) and beach characteristics ( $\beta, K_s$ ). Therefore, rough/smooth beds and different frequency spread values were used to assess the effect on runup. Furthermore, simulating 20 realizations for each wave condition and estimating the mean  $\mu$  and standard deviation  $\sigma$  of the different components of  $R_{2\%}$  allow us to address the role of aleatory uncertainty. Each series of tests (i.e., NB\_S, NB\_R, and BB\_R) corresponds to different spectra and bed characteristics. For instance, NB\_S corresponds to the control case with a Narrow Band spectrum ( $\gamma = 3.3$ ) and Smooth bed, whereas the effect of frequency spread and bed characteristics can be determined from the comparison of the control case with respect to the Broad Band and Rough bed (BB\_R) and the Narrow Band and Rough bed (NB\_R), respectively. Two different bed slope values (1:10 and 1:20) were considered to extend the surf similarity parameter space.

**Table 1** Model skill  $\theta_{skill}$  for wave runup predictions of the simulated cases

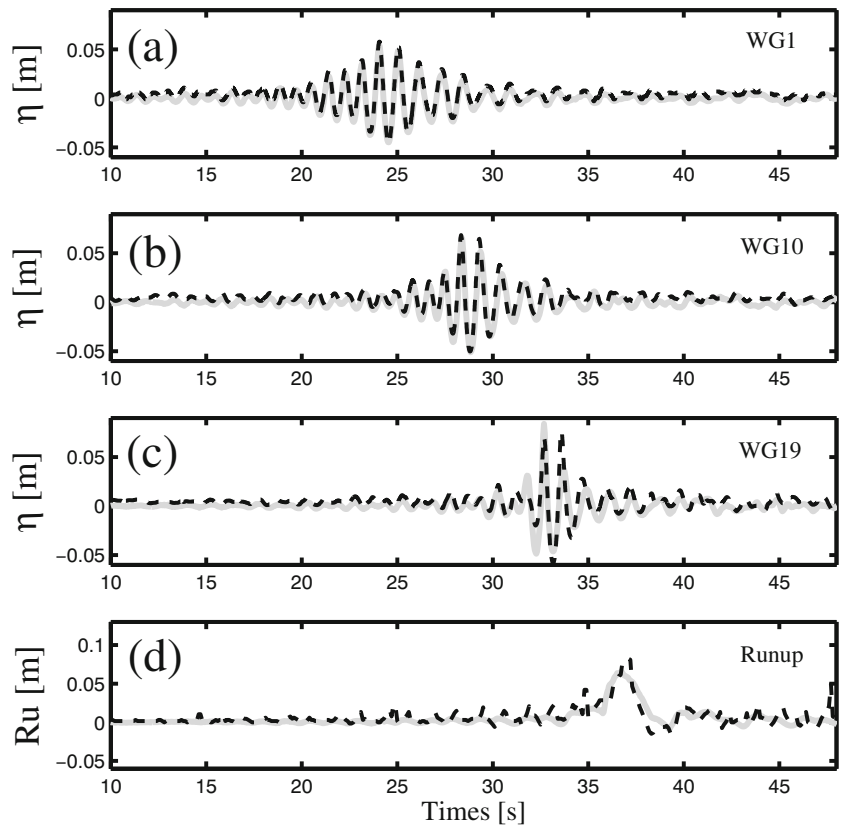
$H$ (m)	$T$ (s)	$\xi_0$	$\theta_{skill}$
0.0212	10	8.84	0.995
0.046	5	2.79	0.971
0.05	4	2.23	0.973
0.05	3	1.68	0.915

**3 Methods**

**3.1 Random wave forcing**

The numerical model requires free surface elevation time series in order to derive the forcing condition following 2.2.

**Fig. 3** Model-data (data: black dashed curve; model: gray solid curve) comparison of **a–c** wave transformation and **d** wave runup for a transient wave group. Laboratory data correspond to the experiments conducted by Baldock (2006)



Thus, synthetic free-surface time series were obtained from a JONSWAP wave energy density spectrum (Hasselmann et al. 1973) using,

$$S(\omega) = \beta_J H_s^2 T_p^{-4} \omega^{-5} \exp \left[ -1.25(T_p \omega)^{-4} \right] \times \gamma \exp \left[ -(T_p \omega - 1)^2 / 2\sigma^2 \right] \tag{9}$$

$$\beta_J = \frac{0.0624}{0.23 + 0.0336\gamma - 0.185(1.9 + \gamma)^{-1} \times [1.094 - 0.01915 \ln \gamma]} \tag{10}$$

$$T_p \approx T_{1/3} \left[ 1 - 0.132(\gamma + 0.2)^{-0.559} \right] \tag{11}$$

$$\sigma \approx \begin{cases} 0.07 & : \omega \leq \omega_p \\ 0.09 & : \omega \geq \omega_p \end{cases} \tag{12}$$

**Table 2** Simulated series: (i) NB\_S corresponds to a narrow band spectrum transformation on a smooth bed; (ii) NB\_R represent narrow band spectrum on a rough bed; and (iii) BB\_R represent broad band spectra on a rough bed

Series	$\gamma$	$K_s$
NB_S	3.3	---
NB_R	3.3	0.0022
BB_R	1.0	0.0022

where  $w$  is the wave frequency,  $w_p$  represents peak wave-frequency,  $\gamma$  is the peak enhancement factor,  $\sigma$  is the peak shape factor,  $H_s$  is the significant wave height,  $T_{1/3}$  is the period associated to  $H_s$ , and  $T_p$  is the spectral peak period. The wave characteristics employed for the simulated cases are shown in Table 3.

Monte Carlo simulations were employed for the estimation of random phases in order to generate 20 different realizations from the wave spectral conditions via an inverse Fourier transform using,

$$\eta = \sum_{i=1}^N \frac{H_i}{2} \cos(-\omega_i t + \psi_i) \tag{13}$$

**Table 3** Wave characteristics at  $h = 0.8$  m of the simulated cases in series NB\_S, NB\_R, and BB\_R

Case	$H_s$ (m)	$T_p$ (s)	$\beta$	$\beta(H_s L_p)^{1/2}$
1	0.10	1.5	0.05	0.028
2	0.15	2.0	0.05	0.043
3	0.20	3.3	0.05	0.066
4	0.07	1.5	0.05	0.024
5	0.20	3.3	0.10	0.133
6	0.15	3.3	0.10	0.115
7	0.10	3.3	0.10	0.094
8	0.07	3.3	0.10	0.078

where  $k$  is the wave number,  $H$  is the wave height, and  $\psi$  the phase of the  $i$ th wave component of the irregular wave spectrum.

Free-surface elevation time series corresponding to different realizations for the same JONSWAP spectrum are shown in Fig. 4. The length of the time series is set equal to 245 s that corresponds to approximately 100 waves, consistent with the duration of data series typically employed for computing runup statistics from field data (e.g., Stockdon et al. 2006; Hughes et al. 2014). The numerical model is forced with free-surface elevation time series using second-order wave theory for deriving the velocity profile at the forcing boundary according to (3)–(6).

### 3.2 Data analysis

The runup signal from each simulated case was decomposed into the setup and swash contribution (e.g., Stockdon et al. 2006). The swash is further decomposed into low-frequency (lf) and high-frequency (hf) swash, obtained by using the low-/high- passed filtered signal of the swash data, respectively. The threshold between hf and lf was set equal to  $f_p/2$  (Janssen et al. 2003). For each case, the ensemble average and the standard deviation of different parameters result from the 20 independent realizations. A sensitivity test was carried out to determine the minimum number of realizations for obtaining ensemble statistics of the different runup parameters. Ensemble averages and standard deviation for the mean shoreline elevation (setup), incident and infragravity swash height, and  $R_{2\%}$  were computed as a function of the number realizations (Fig. 5; example from BB\_R7). The sensitivity analysis suggests that 20 realizations provide reliable estimates for the shoreline elevation, incident and infragravity swash height, and  $R_{2\%}$  for all cases. Notice that the maximum runup (gray circles

in Fig. 5) did not converge over 20 realizations as maximum runup is not a statistical quantity or the product of time averaging and hence requires a larger number of realizations (see Williams et al. 2014). Sensitivity tests for the other cases yielded similar results.

## 4 Results

### 4.1 Runup variability

Runup time series for the simulated cases (Table 2) were employed to investigate the  $R_{2\%}$  variability associated with different parameters including the wave forcing ( $H_s$ ,  $T_p$ ,  $\gamma$ ), the bed characteristics ( $K_s$ ,  $\tan\beta$ ), and the aleatory uncertainty. The  $R_{2\%}$  components were compared with the Hunt scaling parameter (Hunt 1959) (i.e.,  $\beta(H_s L_p)^{1/2}$ ). The results from all cases and realizations show scatter (see Fig. 6), becoming the largest for the  $S_{lf}$  component (Fig. 6c) and the smallest for the setup. This results highlight the difficulties of comparing runup parameterizations with measured data. Thus, ensemble averaging of the realizations was conducted for each case to diagnose the sources of runup variability (Fig. 7). Differences between ensemble results provide a reliable assessment of the influence that different forcing/beach characteristics has on runup, whereas the standard deviation provides a means to estimate the aleatory variability intrinsic to the runup process. The  $R_{2\%}$  variability presented in Fig. 6a is represented in terms of ensemble estimates, as shown in Fig. 7. In general, the aleatory uncertainty, represented by the error bars, is of the same order as the variability induced by differences in the wave spectral or bed characteristics. This implies that natural variability contribution cannot be neglected.

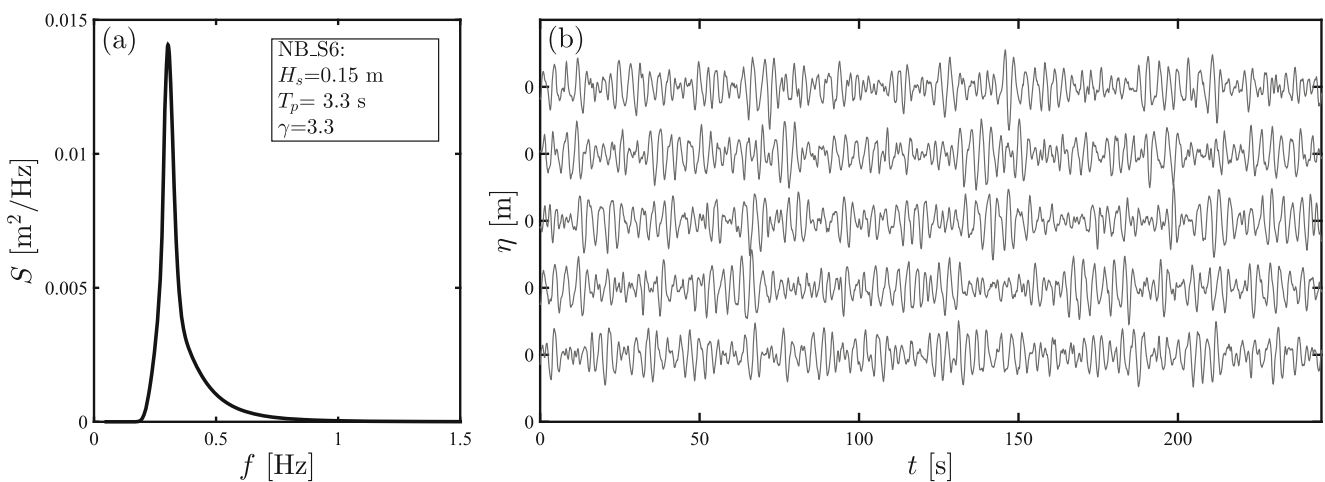


**Fig. 4** **a** JONSWAP wave density spectrum and **b** examples of different realizations corresponding to NB\_S6 ( $H_s=0.15$  m,  $T_p= 3.3$  s, and  $\gamma=3.3$ )

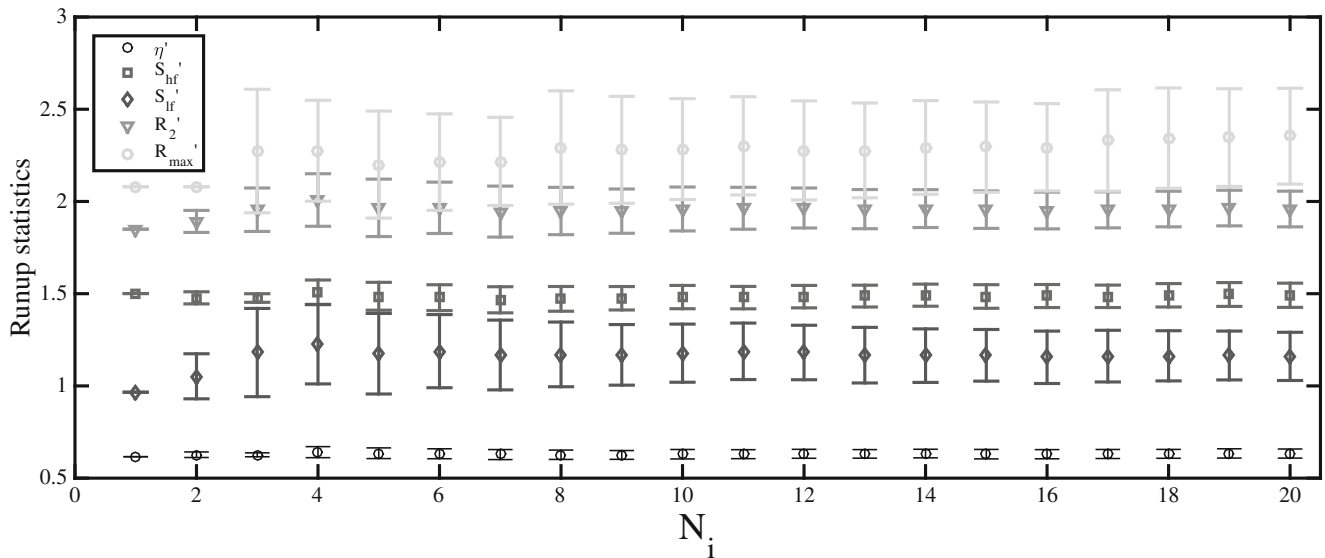


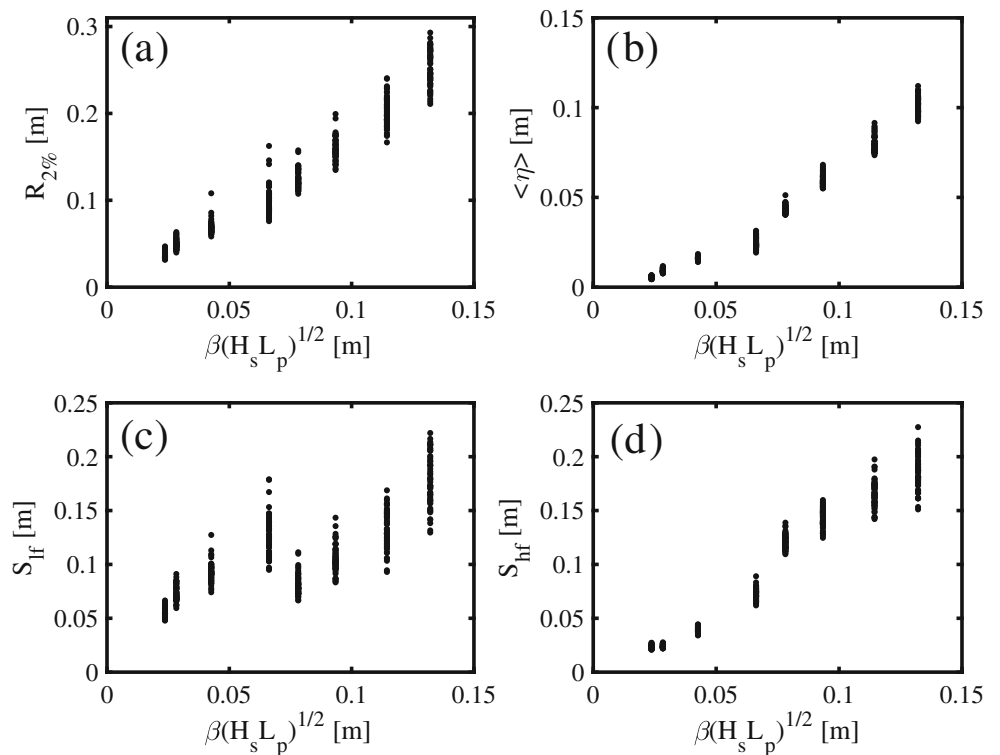
**Fig. 5** Normalized ensemble (average: symbols;  $\pm 1$  standard deviation: error bars) runup statistics with respect to  $H_s$  as a function of the number of realizations. Wave setup (black circles), incident swash

height (black squares), infragravity swash height (black diamonds),  $R_{2\%}$  (gray triangles), and maximum runup (gray circles). Example shown for BB\_R7 ( $H_s = 0.10$  m and  $T_p = 3.3$  s)

Series NB\_R and BB\_R are compared with the idealized cases in series NB\_S to investigate the sources of variability (Fig. 8). NB\_R and BB\_R show an increase and decrease in the  $R_{2\%}$  with respect to NB\_S (Fig. 8a), respectively. Differences between NB\_R and BB\_R become significant for the low-frequency swash contribution (Fig. 8c). Thus, non-linear interaction seems to play an important role

in such differences. On the other hand, increasing the bed roughness and keeping the same frequency spreading (NB\_R) decreases the high frequency swash, owing to increased bed-induced energy losses (Fig. 8d). The mean shoreline elevation is less sensitive than other parameters (Fig. 8b), but is more sensitive to frequency spreading than bed roughness.

**Fig. 6** Numerical results (all cases) of: **a** extreme runup  $R_{2\%}$ , **b** maximum wave setup, **c** lf significant swash height, and **d** hf significant swash height





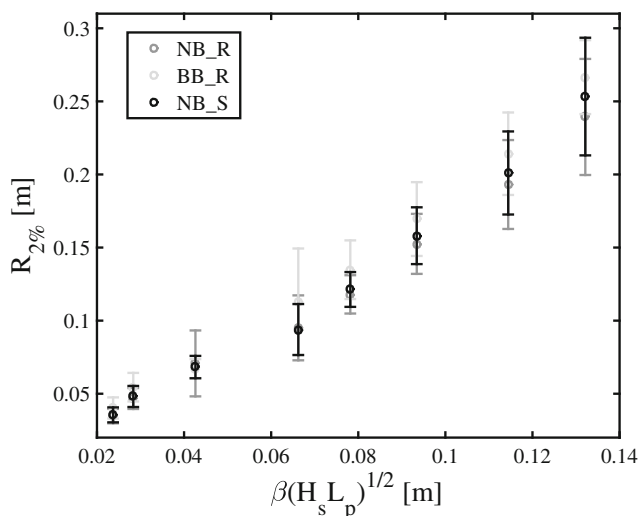


**Fig. 7** Runup ensemble prediction (ensemble averaged: symbols;  $\pm 1$  standard deviation: error bars) of extreme runup  $R_{2\%}$  for the different series

### 4.2 Implications of uncertainty on runup parameterizations

The model results suggest that aleatory uncertainty can be more important than other sources of variability such

as the bed roughness and frequency spread (see Figs. 7 and 8). Therefore, questions arise on both the inherent limitations of current runup parameterizations and the convenience of introducing more parameters into the current  $R_{2\%}$  formulations for reliable estimations of inundation under extreme events. The analysis of the normalized  $R_{2\%}$  corresponding to the realizations for idealized conditions (NB\_S) shows a good fit with a Gaussian Probability Density Function and Cumulative Density Function distributions (Fig. 9). This behavior allows an estimate of the percentage of occurrence as a function of the number of standard deviations  $N_\sigma$  with respect to the ensemble mean value. Here, a new parameterization for  $R_{2\%}$  is proposed, based on the zero intercept of the ensemble average of the realizations under idealized conditions (NB\_S), where the natural (aleatory) uncertainty can be accounted for in terms of the standard deviation. The parameterization is given by,

$$R_{2\%} = [1.76 \pm 0.19N_\sigma] \beta (H_0 L_0)^{1/2} \tag{14}$$

where  $N_\sigma=1, 2, 3, \dots$  and the  $H_0$  and  $L_0$  are deep water wave height and wavelength. By comparing (14) with the results from all simulations (see Fig. 10), it is found that more than 56%, 86%, and 95% of the data are contained within  $N_\sigma = 1, 2,$  and 3 standard deviations, respectively.

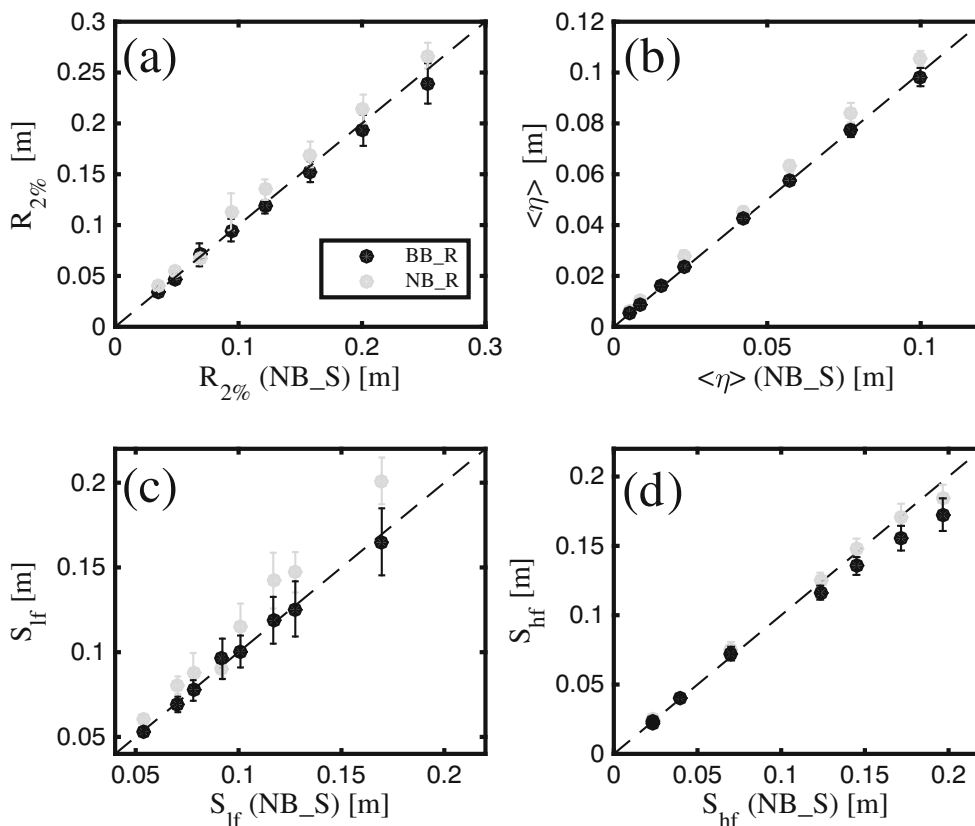


**Fig. 8** Effect of bed roughness (NB\_R) and frequency spread (BB\_R) on runup with respect to the reference condition (NB\_S): **a** extreme runup; **b** shoreline elevation; **c** lf significant swash; and **d** hf significant

swash. The symbols represent the ensemble average, the error bars represent  $\pm 1$  standard deviation) and the dashed line represents perfect agreement with the reference conditions

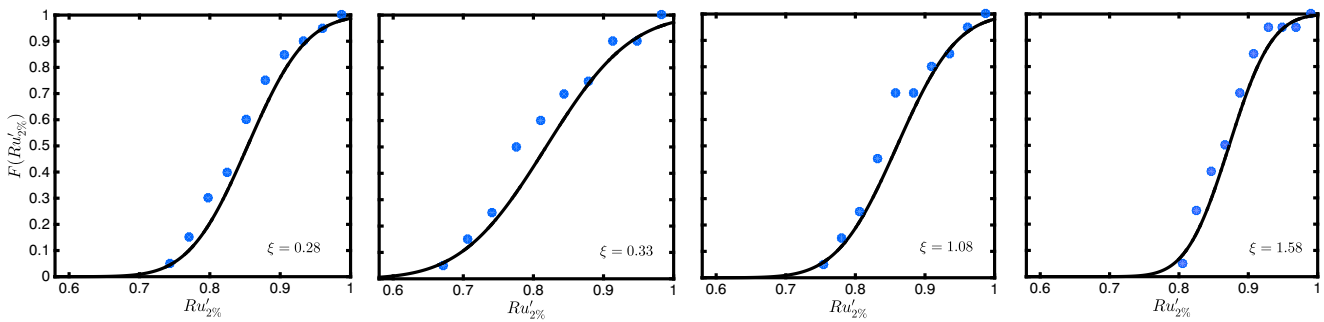


**Fig. 9** Normal distribution fit (black solid curve) to the normalized extreme runup  $Ru'_{2\%}$  (blue circles) for all realizations in cases with different  $\xi$ : **a** NB\_R1, **b** NB\_R3, **c** NB\_R6 and **d** NB\_R8

This implies that accounting for the variability associated with the aleatory uncertainty can be more important than considering other sources of variability (e.g., frequency spread and bed roughness).

### 5 Discussion

Runup models are derived from the laboratory and field observations, and numerical model predictions. The differences in the runup prediction between models are site-dependent and hence might not be applicable to other sites (Atkinson et al. 2017). Atkinson et al. (2017) investigated the performance of 11 runup models, derived in prior laboratory and field studies, for different beaches along the Australian East coast and derived a model-of-models through a least-squares fit as,

$$R_{2\%} = 0.99\beta(H_s L_p)^{1/2} \tag{15}$$

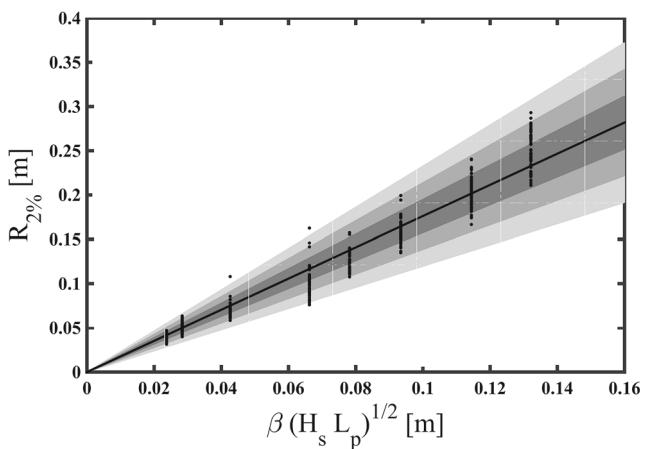


**Fig. 10** Extreme runup  $R_{2\%}$  parameterization for the ensemble average of the smooth bed case (NB\_S) accounting for the aleatory uncertainty (fit to the ensemble results: solid line;  $\pm 1$  standard deviation limit: dark gray shading area;  $\pm 2$  standard deviations limit: medium gray shading area;  $\pm 3$  standard deviations limit: light gray shading area; dots: results from all the realizations)

where the runup coefficient is 0.99, which is almost exactly the same as Holman (1986), and hence implies that  $R_{2\%}$  can be well predicted by the Hunt (1959) scaling parameter. The ensembled parametric model derived in the present work (14) yielded a runup coefficient of 1.76 which is 78% larger. However, the runup coefficient in (14) is consistent with the one derived using runup data in a wave flume (van der Meer and Stam 1992). The differences between (15) and 2D (flume and numerical) data suggests that 3D effects (angular spreading), not accounted in the numerical model and wave flume experiments, might play an important role in decreasing the runup on natural beaches (Guza and Feddersen 2012). An assessment of 3D effects is beyond of the scope of the present investigation and hence further research is warranted.

We investigate the increase in runup variability for some cases (see Fig. 10). The relative runup variability  $\sigma' = \sigma/\mu$ , where  $\mu$  and  $\sigma$  represent the ensemble mean and standard deviation is estimated for all simulated cases to investigate the role of beach slope and wave conditions. Figure 11 shows how the relative runup variability increases for decreasing  $\xi$  values. This suggests that runup variability is

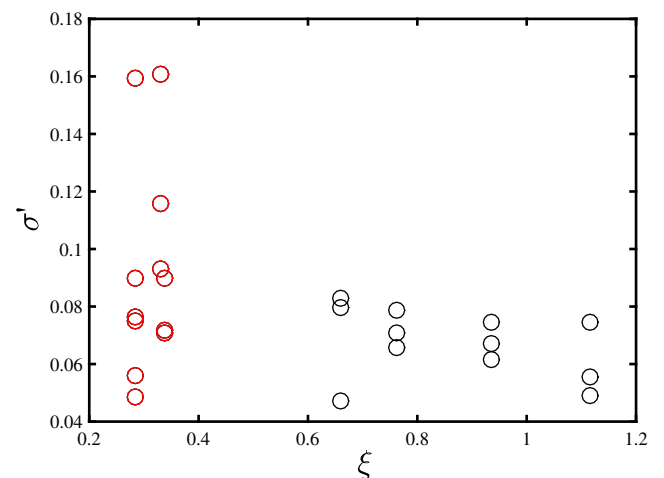


**Fig. 11** Relative runup variability as a function of the surf similarity parameter and bed slope (red circles:  $\beta = 0.05$ ; black circles:  $\beta = 0.1$ )

larger on dissipative beaches ( $\xi < 0.3$ ). The variability can be ascribed to the low-frequency energy contribution which shows the largest scatter (Fig. 6) and tends to dominate the swash in such environments (Stockdon et al. 2006).

## 6 Conclusions

A deterministic model is employed to obtain stochastic runup predictions based on the ensembles of multiple realizations with constant spectral conditions. Ensemble estimates of extreme runup and its different components are computed for different values of frequency spread and bed roughness. Numerical results suggest that the setup and the low-frequency significant swash height are more sensitive to frequency spreading than bed roughness. On the other hand, the high-frequency significant swash is more sensitive to bed roughness. Nevertheless, the model simulations of  $R_{2\%}$  show that the variability ascribed to different frequency spread and bed roughness values are within the uncertainty values of the idealized condition. A new parameterization for  $R_{2\%}$  that incorporates the aleatory uncertainty accounts for 95% of all the cases considering variability within 3 standard deviations, irrespective of the bed roughness and frequency spread values. These results suggest that current parameterization needs to incorporate aleatory uncertainty for reliable predictions of extreme events.

**Acknowledgments** We acknowledge Gonzalo Uriel Martín Ruiz for technical support. The first author acknowledge Dr. Jantine Rutten for discussion on the assessment of relative runup variability. Two anonymous reviewers provided valuable comments that improved the manuscript.

**Funding information** We acknowledge ONR Global and CONACYT (CB-2016-284430 and LN 271544) for financial support. Additional financial support was provided by UNAM through PAPIIT DGAPA (PAPIIT IN101218) and the International Collaborative Project between Instituto de Ingeniería and the University of Delaware. J.C. Pintado-Patiño acknowledges the financial support provided by the Mexican National Council of Science and Technology (CoNACyT) under the graduate scholarship 490080.

## References


- Apotsos A, Raubenheimer B, Elgar S, Guza RT (2008) Wave-driven setup and alongshore flows observed onshore of a submarine canyon. *J Geophys Res* 113(C07025)
- Atkinson AL, Power HE, Moura T, Hammond T, Callaghan DP, Baldock TE (2017) Assessment of runup predictions by empirical models on non-truncated beaches on the south-east australian coast. *Coast Eng* 119:15–31. <https://doi.org/10.1016/j.coastaleng.2016.10.001>. <http://www.sciencedirect.com/science/article/pii/S037838391630285X>
- Baldock T, Holmes P (1999) Simulation and prediction of swash oscillations on a steep beach. *Coast Eng* 36(3):219–242. [https://doi.org/10.1016/S0378-3839\(99\)00011-3](https://doi.org/10.1016/S0378-3839(99)00011-3). <http://www.sciencedirect.com/science/article/pii/S0378383999000113>
- Baldock TE (2006) Long wave generation by the shoaling and breaking of transient wave groups on a beach. *Proc R Soc A* 462:1853–1876
- Baldock TE, Huntley DA (2002) Long wave forcing by the breaking of random gravity waves on a beach. *Proc R Soc A* 458:2177–2201
- Baldock TE, Swan C, Taylor PH (1996) A laboratory study of non-linear surface waves on water. *Phil Trans R Soc A* 354:649–676
- Baldock TE, Huntley DA, Bird PAD, O'Hare TJ, Bullock GN (2000) Breakpoint generated surf beat induced by bichromatic wave groups. *Coast Eng* 39:213–242
- Baldock TE, Perris D, Hogg AJ (2012) Overtopping of solitary waves and solitary bores on a plane beach. *Proc R Soc A* 468:3494–3516
- Battjes JA (1974) Surf similarity. In: Proceedings of the 14th international conference on coastal eng, ASCE
- Briganti R, Torres-Freyermuth A, Baldock TE, Brocchini M, Dodd N, Hsu T, Jiang Z, Kim Y, Pintado-Patio JC, Postacchini M (2016) Advances in numerical modelling of swash zone dynamics. *Coast Eng* 115:26–41. <https://doi.org/10.1016/j.coastaleng.2016.05.001>
- Brinkkemper JA, Torres-Freyermuth A, Mendoza ET, Ruessink BG (2013) Parameterization of wave run-up on beaches in Yucatan, Mexico: a numerical study. In: Coastal dynamics, pp 225–234
- Desombre J, Morichon D, Mory M (2013) {RANS} v2f simulation of a swash event: detailed flow structure. *Coast Eng* 71:1–12. <https://doi.org/10.1016/j.coastaleng.2012.07.001>. <http://www.sciencedirect.com/science/article/pii/S0378383912001342>
- Didenkulova I, Didenkulov O, Pelinovsky E (2015) A note on the uncertainty in tsunami shape for estimation of its run-up heights. *Journal of Ocean Engineering and Marine Energy* 1(2):199–205. <https://doi.org/10.1007/s40722-015-0017-3>
- Fiedler JW, Smit PB, Brodie KL, McNinch J, Guza R (2019) The offshore boundary condition in surf zone modeling. *Coast Eng* 143:12–20. <https://doi.org/10.1016/j.coastaleng.2018.10.014>. <http://www.sciencedirect.com/science/article/pii/S0378383918301984>
- Fitzgerald CJ, Taylor PH, Orszaghova J, Borthwick AG, Whittaker C, Raby AC (2016) Irregular wave runup statistics on plane beaches: Application of a Boussinesq-type model incorporating a generating absorbing sponge layer and second-order wave generation. *Coast Eng* 114:309–324. <https://doi.org/10.1016/j.coastaleng.2016.04.019>. <http://www.sciencedirect.com/science/article/pii/S0378383916300667>
- Ge L, Cheung K (2011) Spectral sampling method for uncertainty propagation in long-wave runup modeling. *J Hydraulic Eng* 137:277–288
- Guza RT, Feddersen F (2012) Effect of wave frequency and directional spread on shoreline runup. *Geophys Res Lett* 39(L11607). <https://doi.org/10.1029/2012GL051959>
- Guza RT, Thornton EB (1982) Swash oscillations on a natural beach. *J Geophys Res Oceans* 87(C1):483–491. <https://doi.org/10.1029/JC087iC01p00483>
- Hasselmann K, Barnett T, Bonws E, Carlson H, Cartwright DC, Enke K, Ewing J, Gienapp H, Hasselmann DE, Kruseman P, Meerburg A, Muller P, Olbers DJ, Richter K, Sell W, Walden H (1973) Measurements of wind-wave growth and swell decay during the joint north sea wave project (jonswap). Tech. Rep. Tech. rep, Deutsches Hydrographisches Institut
- Hirt CW, Nichols BD (1990) Volume of fluid (VOF) method for dynamics of free boundaries. *J Comput Phys* 39:201–225
- Holland KT, Raubenheimer B, Guza RT, Holman RA (1995) Runup kinematics on a natural beach. *J Geophys Res Oceans* 100(C3):4985–4993. <https://doi.org/10.1029/94JC02664>
- Holman RA (1986) Extreme value statistics for wave run-up on a natural beach. *Coast Eng* 9(6):527–544

- Sallenger AH (1985) Setup and swash on a natural beach. *J Geophys Res Oceans* 90(C1):945–953. <https://doi.org/10.1029/JC090iC01p00945>
- Hsu TJ, Sakakiyama T, Liu PLF (2002) A numerical model for wave motions and turbulence flows in front of a composite breakwater. *Coastal Eng* 46:25–50
- Hsu TJ, Elgar S, Guza RT (2006) Wave-induced sediment transport and onshore sandbar migration. *Coastal Eng* 53:817–824
- Hughes MG, Aagaard T, Baldock TE, Power HE (2014) Spectral signatures for swash on reflective, intermediate and dissipative beaches. *Marine Geology* 355:88–97. <https://doi.org/10.1016/j.margeo.2014.05.015>. <http://www.sciencedirect.com/science/article/pii/S0025322714001492>
- Hunt IA (1959) Design of seawalls and breakwaters. *J Waterw Port Coastal Ocean Eng* 85:123–152
- Janssen TT, Battjes JA, van Dongeren AR (2003) Long waves induced by short-wave groups over a sloping bottom. *J Geophys Res* 108(C8):3252. <https://doi.org/10.1029/2002JC001515>
- Lara JL, Ruju A, Losada IJ (2011) Reynolds averaged Navier-Stokes modelling of long waves induced by a transient wave group on a beach. *Proceedings of the Royal Society of London A: Mathematical, Physical and Engineering Sciences* 467(2129):1215–1242. <https://doi.org/10.1098/rspa.2010.0331>. <http://rspa.royalsocietypublishing.org/content/467/2129/1215>
- Lin P, Liu PLF (1998) A numerical study of breaking waves in the surf zone. *J Fluid Mech* 359:239–264
- Longuet-Higgins MS, Stewart R (1960) Change in the form of short gravity waves on long waves and tidal currents. *J Fluid Mech* 8:565–583
- Losada IJ, Lara JL, Guanche R, González-Ondina JM (2008) Numerical analysis of wave overtopping of high mound breakwaters. *Coastal Eng* 55:47–62. <https://doi.org/10.1016/j.coastaleng.2007.06.003>
- Madsen PA, Sorensen OR, Schaffer HA (1997) Surf zone dynamics simulated by a Boussinesq type model: I. model description and cross-shore motion of regular waves. *Coastal Eng* 32:255–287
- Medellin G, Brinkkemper JA, Torres-Freyermuth A, Appending CM, Mendoza ET, Salles P (2016) Run-up parameterization and beach vulnerability assesment on a barrier island: a downscaling approach. *Nat Hazards Earth Syst Sci* 16:167–180
- van der Meer JW, Stam CM (1992) Wave runup on smooth and rock slopes of coastal structures. *J Waterw Port Coastal Ocean Eng* 118(5):534–550. [https://doi.org/10.1061/\(ASCE\)0733-950X\(1992\)118:5\(534\)](https://doi.org/10.1061/(ASCE)0733-950X(1992)118:5(534))
- Palemón-Arcos L, Torres-Freyermuth A, Pedrozo-Acuña A, Salles P (2015) On the role of uncertainty for the study of wave-structure interaction. *Coast Eng* 106:32–41. <https://doi.org/10.1016/j.coastaleng.2015.09.005>. <http://www.sciencedirect.com/science/article/pii/S0378383915001532>
- Palmsten ML, Splinter KD (2016) Observations and simulations of wave runup during a laboratory dune erosion experiment. *Coast Eng* 115:58–66. <https://doi.org/10.1016/j.coastaleng.2016.01.007>. <http://www.sciencedirect.com/science/article/pii/S037838391600017X>, swash-zone Processes
- Park H, Cox DT (2016) Empirical wave run-up formula for wave, storm surge and berm width. *Coast Eng* 115:67–78. <https://doi.org/10.1016/j.coastaleng.2015.10.006>. <http://www.sciencedirect.com/science/article/pii/S0378383915001830>, swash-zone processes
- Pintado-Patiño JC, Torres-Freyermuth A, Puleo JA, Pokrajac D (2015) On the role of infiltration and exfiltration in swash zone boundary layer dynamics. *J Geophys Res* 120:6329–6350
- Poate TG, McCall RT, Masselink G (2016) A new parameterisation for runup on gravel beaches. *Coast Eng* 117:176–190. <https://doi.org/10.1016/j.coastaleng.2016.08.003>. <http://www.sciencedirect.com/science/article/pii/S0378383916301697>
- Ricchiuto M, Congaed PM, Delis AI (2014) Runup and uncertainty quantification: sensitivity analysis via anova decomposition. *Tech. Rep. Res. Rep.RR-8530*, INRIA
- Rodi W (1993) Turbulence models and their application in hydraulics—a-state-of-the-art review. *Int. Assoc. for Hydraul. Res., Delft, Netherlands*
- Rodriguez-Rincon JP, Pedrozo-Acuña A, Breña-Naranjo JA (2015) Propagation of hydro-meteorological uncertainty in a model cascade framework to inundation prediction. *Hydrol Earth Syst Sci* 19:2981–2998
- Romano A, Bellotti G, Briganti R, Franco L (2015) Uncertainties in the physical modelling of the wave overtopping over a rubble mound breakwater: The role of the seeding number and of the test duration. *Coast Eng* 103:15–21. <https://doi.org/10.1016/j.coastaleng.2015.05.005>. <http://www.sciencedirect.com/science/article/pii/S0378383915000915>
- Ruessink BG, Kleinhan MG, van den Beukel PGL (1998) Observations of swash under highly dissipative conditions. *J Geophys Res Oceans* 103(C2):3111–3118. <https://doi.org/10.1029/97JC02791>
- Ruggiero P, Holman RA, Beach RA (2004) Wave run-up on a high-energy dissipative beach. *J Geophys Res Oceans* 109(C6):n/a–n/a. <https://doi.org/10.1029/2003JC002160>, c06025
- Ruju A, Lara JL, Losada IJ (2014) Numerical analysis of run-up oscillations under dissipative conditions. *Coast Eng* 86:45–56. <https://doi.org/10.1016/j.coastaleng.2014.01.010>. <http://www.sciencedirect.com/science/article/pii/S0378383914000192>
- Sallenger AH (2000) Storm impact scale for barrier island. *J Coast Res* 16(3):890–895
- Stockdon H, Thompson D, Plant N, Long J (2014) Evaluation of wave runup predictions from numerical and parametric models. *Coast Eng* 92:1–11. <https://doi.org/10.1016/j.coastaleng.2014.06.004>. <http://www.sciencedirect.com/science/article/pii/S0378383914001239>
- Stockdon HF, Holman RA, Howd PA, Sallenger AH Jr (2006) Empirical parameterization of setup, swash, and runup. *Coast Eng* 53(7):573–588. <https://doi.org/10.1016/j.coastaleng.2005.12.005>. <http://www.sciencedirect.com/science/article/pii/S0378383906000044>
- Stockdon HF, Sallenger AH, Holman RA, Howd PA (2007) A simple model for the spatially-variable coastal response to hurricanes. *Mar Geol* 238(1):1–20. <https://doi.org/10.1016/j.margeo.2006.11.004>. <http://www.sciencedirect.com/science/article/pii/S0025322706003355>
- Torres-Freyermuth A, Lara JL, Losada IJ (2010) Numerical modelling of short- and long-wave transformation on a barred beach. *Coastal Eng* 57(3):317–330. <https://doi.org/10.1016/j.coastaleng.2009.10.013>
- Torres-Freyermuth A, Puleo JA, Pokrajac D (2013) Modeling swash-zone hydrodynamics and shear stresses on planar slopes using Reynolds-averaged Navier–Stokes equations. *J Geophys Res Oceans* 118(2):1019–1033. <https://doi.org/10.1002/jgrc.20074>
- Williams HE, Briganti R, Pullen T (2014) The role of offshore boundary conditions in the uncertainty of numerical prediction of wave overtopping using non-linear shallow water equations. *Coast Eng* 89:30–44. <https://doi.org/10.1016/j.coastaleng.2014.03.003>. <http://www.sciencedirect.com/science/article/pii/S0378383914000568>
- Willmott CJ, Ackleson SG, Davis RE, Feddema JJ, Klink KM, Legates DR, O’Donnell J, Rowe CM (1985) Statistics for the evaluation and comparison of models. *J Geophys Res Oceans* 90(C5):8995–9005. <https://doi.org/10.1029/JC090iC05p08995>

Zhang Q, Liu PLF (2008) A numerical study of swash flows generated by bores. *Coastal Eng* 55(12):1113–1134. <https://doi.org/10.1016/j.coastaleng.2008.04.010>

Zijlema M, Stelling G, Smit P (2011) Swash: an operational public domain code for simulating wave fields and rapidly varied flows in coastal waters. *Coast Eng* 58(10):992–1012. <https://doi.org/10.1016/j.coastaleng.2011.05.015>. <http://www.sciencedirect.com/science/article/pii/S0378383911000974>

## Affiliations

Alec Torres-Freyermuth<sup>1</sup>  · Jose Carlos Pintado-Patiño<sup>2</sup> · Adrián Pedrozo-Acuña<sup>3</sup> · Jack A. Puleo<sup>4</sup> · Tom E. Baldock<sup>5</sup>

Jose Carlos Pintado-Patiño  
jose.pintado@enesmerida.unam.mx

Adrián Pedrozo-Acuña  
APedrozoA@iingen.unam.mx

Jack A. Puleo  
jpuleo@udel.edu

Tom E. Baldock  
t.baldock@uq.edu.au

<sup>1</sup> Instituto de Ingeniería, Universidad Nacional Autónoma de México, Puerto de Abrigo s/n, Sisal, YU 97356, México

<sup>2</sup> Escuela Nacional de Estudios Superiores, Unidad Mérida, Universidad Nacional Autónoma de México, Carretera Mérida-Tetiz, Km 4, Ucu, YU 97357, México

<sup>3</sup> Instituto de Ingeniería, Universidad Nacional Autónoma de México, Circuito Escolar s/n, Ciudad Universitaria, Delegación Coyoacán, CDMX 04510, México

<sup>4</sup> Center for Applied Coastal Research, University of Delaware, Newark, DE 19716, USA

<sup>5</sup> School of Civil Engineering, University of Queensland, St Lucia, QLD 4072, Australia